Neuro-Oncology Advances
7(1), vdaf045, 2025 | https://doi.org/10.1093/noajnl/vdaf045 | Advance Access date 25 February 2025

Effects of craniectomy defect on tumor-treating fields

Edwin Lok[‡], Bryant Chang[‡], Rafael Vega, Monika Haack, and Eric T. Wong

All author affiliations are listed at the end of the article

Corresponding Author: Eric T. Wong, MD, MA, Division of Hematology/Oncology, Rhode Island Hospital, George 315, 593 Eddy Street, Providence, RI 02903, USA (ewong1@brownhealth.org); Edwin Lok, MS, Division of Hematology/Oncology, Rhode Island Hospital, George 315, 593 Eddy Street, Providence, RI 02903, USA (elok@bidmc.harvard.edu).

[‡]Contributed equally.

Abstract

Background. Tumor-treating fields (TTFields) are alternating electric fields approved for the treatment of glioblastoma. They must penetrate through the skull to reach the gross tumor volume (GTV) in the brain. Since the skull is an attenuator of electric fields, removal of a section of cortical bone by craniectomy may facilitate the delivery of TTFields into the GTV.

Methods. We identified a glioblastoma patient who underwent craniectomy for evacuation of a subdural empyema. The patient subsequently received standard adjuvant treatment with TTFields plus temozolomide without replacement of the skull defect. Post-acquisition magnetic resonance imaging datasets were obtained from this index patient and 2 others for virtual craniectomy analysis. After anatomic delineation, a 3-dimensional finite element mesh was generated and then solved for the distribution of applied electric fields, rate of energy deposition, and current density at the GTV.

Results. The geometry of craniectomy defect alone, with or without burr holes, did not alter TTFields delivery to GTV. Biomaterials filling the defect could significantly influence electric field penetration, particularly when they are highly conductive at 10 S/m or 7.76×10^6 S/m as in tantalum. The ratio of GTV relative to defect size also enhanced or attenuated TTFields coverage when the GTV was expanded or eroded, respectively.

Conclusions. Craniectomy, biomaterials filling the defect, and the ratio of GTV relative to defect size may interact in a combinatorial fashion in modulating TTFields penetration into the brain. These findings are clinically relevant for personalized TTFields treatment.

Key Points

1. Biomaterials at the craniectomy defect could influence the penetration of tumor-treating fields.
2. Ratio of gross tumor volume relative to defect size can enhance or attenuate tumor-treating fields.

Tumor-treating fields (TTFields) therapy is a standard of care for patients with glioblastoma.[1,2] This treatment is delivered to the head continuously via 2 pairs of orthogonally positioned transducer arrays.[3] For newly diagnosed glioblastoma patients, randomized clinical trial has shown that when TTFields were added to temozolomide in the adjuvant setting, the combination improved both progression-free and overall survivals compared to temozolomide alone.[4] The only unique adverse event related to TTFields was mild to moderate scalp irritation at the sites of array application.[5] Therefore, this favorable toxicity profile will most likely allow oncologists to adopt a combinatorial approach with other modalities of anti-glioblastoma treatment.

From a biological perspective, the anti-cancer efficacy of TTFields arises from alternating electric fields, tuned to a frequency of 200 kHz, from which a multitude of biological effects are induced, including disruption of tumor cells during mitosis, induction of double-stranded DNA breaks, and

Importance of the Study

Craniectomy has been shown to increase penetration of tumor-treating fields into the brain. However, factors that modulate this effect are unknown. This article documents (i) the biomaterials filling the defect and (ii) the gross tumor volume relative to defect size are 2 important modulators. This knowledge provides a means of optimizing the application of TTFields for glioblastoma.

triggering various cellular stress responses leading to secondary autophagy, immunogenic cell death, or both.[6–9] The effectiveness of TTFields in targeting tumor cells is influenced by the intensity and distribution of electric fields at the tumor site, with the observation that higher field strength correlates with enhanced anti-cancer properties.[10] Since dosimetry of TTFields cannot be solved analytically due to their nonlinear propagation characteristics, finite element analysis is used to approximate the dose at the gross tumor volume (GTV) by computer modeling.[11] Still, propagation and distribution of TTFields are heavily influenced by, but not limited to, local tissue conductance, presence or absence of cerebral edema, neuroanatomic geometry, and structural integrity of the skull.[12–15] Here, we aimed to investigate the impact of skull defect on the distribution and intensity of TTFields at the glioblastoma and adopted the following approaches: First, the shape of the craniectomy defect was examined, since surgical removal of the skull can introduce irregularities in the calvarial geometry, which may disrupt the distribution of TTFields. Additionally, examining the shape of the craniectomy helped to identify configurations that might minimize field disruption. Second, multiple biomaterials were simulated within the defect with various conductivities and characterized how they might intensify or attenuate TTFields at the GTV. Third, the size of the tumor in our models was expanded and contracted, under the hypothesis that larger or smaller tumors might interact differently with electric fields, potentially requiring adjustments of TTFields to achieve optimal coverage. Finally, burr holes in the craniectomy were introduced, since they are often created during neurosurgical procedures, causing additional geometric variations that can affect local conductivity characteristics and the resulting electric field distribution. These burr holes might concentrate or dissipate the fields depending on their size and location, potentially impacting the overall effectiveness of TTFields therapy. By exploring these variables of craniectomy defect, we aimed to maximize field strength at the tumor while minimizing scatter into adjacent healthy tissue, with the ultimate goal of optimizing delivery of TTFields to improve treatment outcomes for glioblastoma patients.

Materials and Methods

Magnetic resonance imaging (MRI) datasets from 3 glioblastoma patients were obtained under an institutional review board-approved protocol at the Dana Farber Cancer Institute. The index patient EY106 (Figure 1) developed a subdural empyema after radiation and daily temozolomide for newly diagnosed glioblastoma and then underwent a craniectomy and evacuation of pus. After successful antibiotics therapy, the patient declined reconstruction or replacement of the skull defect and was subsequently treated with TTFields and adjuvant temozolomide at a dose of 150 to 200 mg/m^2/day for 5 days in 28-day cycles.[4] The treatment-planning MRI revealed that the bone defect was near the site of primary brain tumor resection prior to TTFields, and the MRI dataset was used to segment intracranial structures, GTV, and cerebral edema. The other two patients, CS075 and HE081 (Figure 1), who only received partial resection prior to starting TTFields, were also modeled. Their skull defect shape was introduced virtually according to the dimensions of EY106, which had a diameter of 74.7 mm and a surface area of 80.04 cm^2. Additionally, in all 3 patients, 1-cm burr holes were integrated at the original bone defect, and TTFields coverage at the GTV was compared accordingly with or without them. T1 post-gadolinium, FLAIR, and MP RAGE MR sequences were used to delineate GTV, normal brain tissue compartments, and cerebral edema in the models. A semi-automatic approach described by Timmons, et al. was used to generate a 3-dimensional finite element mesh for each model in ScanIP (Synopsys) and then imported into COMSOL Multiphysics 6.1 (COMSOL) for finite element analysis.[11] Sensitivity analysis as a function of skull defect was performed by varying the electric conductivities based on different biomaterials incorporated for each model (Table 1). The lowest conductive material used in this study was polymethyl methacrylate (PMMA), while the highest was tantalum. Intermediate conductive materials used include cortical bone, fat, titanium, and 2 virtual constructs with a pre-specified conductivity set to 1 and 10 S/m. Additionally, the shape of each model's bone defect was altered by using 7 standard geometric shapes, ranging from circle, triangle, rotated triangle by 90°, square, rotated square by 45°, hexagram, and rotated hexagram by 30° to explore the effects of geometry on the distribution of TTFields. Furthermore, the GTV was expanded as well as eroded to simulate changes in tumor volume relative to the size of the skull defect. For EY106, GTV expansion and erosion were achievable, while for CS075 an erosion model was not possible due to the small size of the original GTV that was used as a reference. For HE081, an expansion model was not feasible because the GTV was too close to the skull base, which prevented uniform expansion.

The electric field distribution for each model was solved using the AC/DC module from COMSOL Multiphysics. Plan quality metrics (PQMs) derived from each model's respective volume histograms were used to make comparisons. PQMs included 95% coverage metrics such as $E_{95\%}$, $SAR_{95\%}$, and $CD_{95\%}$, which correspond to electric field (E) strength,

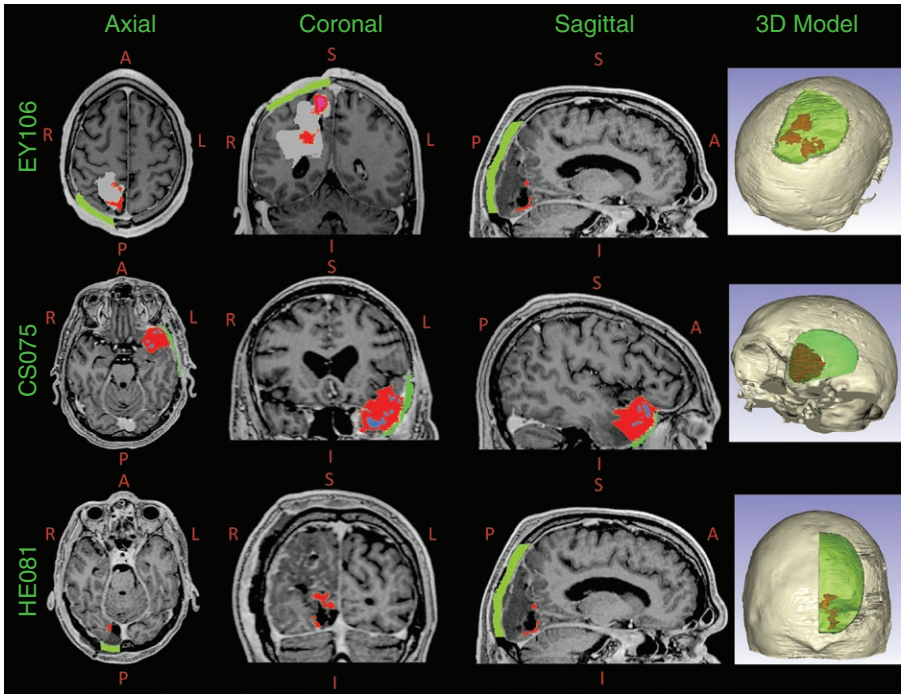

Figure 1. Radiographic images of gross tumor volume (GTV) and skull defects (real and virtual). Axial, coronal, and sagittal post-gadolinium-enhanced T1-weighed images of the GTV (red) are shown for EY106, CS075, and HE081. Computer 3-dimensional rendering of the real skull defect (green) for EY106, as well as the virtual defects (green) for CS075 and HE081, are also displayed. Edema and necrotic core are respectively shown in gray and blue.

Table 1. Electric Conductivity and Density of Biomaterials Filling the Craniectomy Defect

Material Type	Electric conductivity (S/m)	Density (kg/m^3)
PMMA	1.00E – 07	1180
Titanium	1.28E – 06	4506
Cortical bone	2.11E – 02	1908
Fat	4.35E – 02	911
Tantalum	7.70E + 06	16 650

specific absorption rate (SAR; or the rate at which energy is absorbed), and current density (CD), respectively, received by 95% volume of tissue. Median coverage, denoted by $E_{50\%}$, $SAR_{50\%}$, and $CD_{50\%}$, for electric field, SAR, and current density, respectively, were also utilized to quantitatively compare between models. Similarly, 5% hotspot metrics such as $E_{5\%}$, $SAR_{5\%}$, and $CD_{5\%}$ were determined.

Results

Shape of Craniectomy Does Not Significantly Alter Coverage of TTFields in GTV

Coverage of TTFields in the GTV was not significantly altered by changing the shape of each patient model's skull defect (Figure 2) when conserving an equivalent surface area and conductivity of the biomaterial filling the defect (data not shown). When the conductivity was set to 1 S/m, the 30° rotated hexagram was the only shape associated with a large decrease (>10%) in GTV coverage, while other geometries exhibited varying increases of +10% or less.

When comparing the GTV coverage characteristics between each patient's original model of skull defect with and without burr holes, there were varying differences for each of the PQM metrics. The $E_{95\%}$, $E_{50\%}$, and $E_{5\%}$ in EY106 had a minimal difference of –0.2%, –0.2%, and +0.1%, respectively, in the models with burr holes compared to those without. In HE081's GTV, electric field metrics yielded insignificant alteration in coverage of <1%. The GTV of CS075 had virtually no change in coverage (<1%) according to the $E_{95\%}$, $E_{50\%}$ and $E_{5\%}$ metrics. SAR and current density metrics of CS075 and HE081 all exhibited insignificant differences. EY106 had minimal change in current density, $CD_{95\%}$, $CD_{50\%}$, and $CD_{5\%}$ of –0.1%, –0.1%, and +0.1%, respectively. The change in SAR was also minute by –0.2%, –0.3%, and –0.4% for the $SAR_{95\%}$, $SAR_{50\%}$, and $SAR_{5\%}$, respectively. Collectively, in our 3 particular patients, the craniectomy defect with or without burr holes affected GTV coverage only marginally, all within a difference of ±0.5%.

Electric Conductivity of Biomaterials Filling the Craniectomy Defect Affects TTFields Coverage in GTV

Since there were no profound coverage differences observed as a function of defect shape, we then proceeded to examine the biomaterials filling the defect and asked

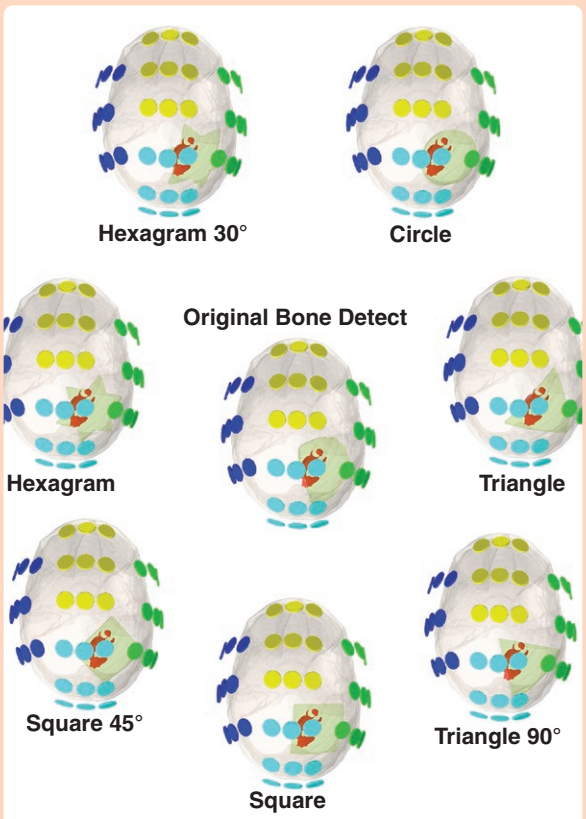

Figure 2. Shapes of craniectomy defect relative to gross tumor volume and electrode arrays. Shapes other than the original craniectomy defect (center) are shown, including circle, triangle without or with 90° rotation clockwise or counterclockwise, square without or with 45° rotation clockwise or counterclockwise, and hexagram without or with 30° rotation clockwise or counterclockwise.

whether their electric conductivity would have an impact on the GTV. We first took the average of all PQM metrics and compared the coverage statistics among cortical bone, PMMA, titanium, and fat (when only the scalp flap is present), all of which are commonly used to fill in the skull defect after a craniectomy and have a conductivity value of <1 S/m (Table 1). Specifically, for EY106, multiple $E_{95\%}$, $CD_{95\%}$, and $SAR_{95\%}$ were all approximately 30 V/m, 8–9 A/m^2, and 0.2 W/kg, respectively (Figure 3A-C). Median coverage metrics such as $E_{50\%}$, $CD_{50\%}$, and $SAR_{50\%}$ were 40–50 V/m, 13–15 A/m^2, and 0.3–0.5 W/kg, respectively. The 5% hotspot metrics, $E_{5\%}$, $CD_{5\%}$, and $SAR_{5\%}$, were 80–90 V/m, 20–25 A/m^2, and 1.2–1.5 W/kg, respectively. In aggregate, fat resulted in the highest coverage and the lowest was found in PMMA. When the defect conductivity was set to 1 S/m, there was a significant reduction in GTV coverage by 10%–20% in the electric field, 20%–40% in SAR, and 15%–20% for current density (Figure 3, A–C). Therefore, we proceeded to examine higher conductivity values, 10 S/m as well as tantalum, which is highly conductive (7.7×10^6 S/m) and a commonly used biomaterial in hip prosthesis. For 10 S/m, there was a further reduction of 20%–90% in electric field, 55%–375% in SAR, and 20%–90% in current density. For tantalum, the reduction was 20%–280% for the electric field, 50%–1330% in SAR, and 30%–270% in current density. These data indicate that PQM metrics were substantially reduced when the conductivity of the biomaterial is above 1 S/m.

To explore further the impact of the conductivity of biomaterials on GTV coverage, we also modeled a virtual defect in HE081 using cortical bone, PMMA, titanium, and fat. Fat on average resulted in the highest coverage and the lowest was found in PMMA. We then proceeded to evaluate prespecified conductivities at 1 and 10 S/m as well as tantalum and revealed a similar but lesser reduction in PQM metrics compared to EY106 (Figure 3, G–I). We further evaluated these changes in CS075 and also found highest coverage from fat and lowest from PMMA (Figure 3, D–F). However, when the biomaterial conductivity was set to 1 S/m, GTV coverage was actually increased by 7%–15% in electric field, 19%–25% in SAR, and 10%–13% for current density. For 10 S/m, there was an increase of 11%–21% in electric field, 18%–35% in SAR, and 12%–21% in current density. For tantalum, the increase was 18%–55% for electric field, 34%–81% in SAR and 18%–53% in current density. Together, there is heterogeneity in PQM metrics among our patients, particularly at conductivity values greater than 1 S/m, and this indicates an additional factor influencing TTFields delivery.

GTV Relative to Size of Skull Defect Affects TTFields Coverage

We hypothesize that the ratio between tumor size and skull defect may also influence TTFields coverage within the GTV. Therefore, to simulate tumor growth, we expanded the GTV while keeping the defect size constant and found that each patient exhibited varying differences in GTV coverage. For EY106, both $E_{95\%}$ and $E_{5\%}$ remained relatively unchanged by +0.9% and +1.1%, respectively, compared to models of the original GTV (Figure 4, A and G), but the $E_{50\%}$ increased by 8.3% (Figure 4D). The $SAR_{95\%}$ decreased by –11.4% (Figure 4B), while both the $SAR_{50\%}$ and $SAR_{5\%}$ increased by +13.8% and +14.7%, respectively (Figure 4, E and H). Similarly, $CD_{95\%}$ decreased by –5.0% (Figure 4C), whereas both $CD_{50\%}$ and $CD_{5\%}$ increased by +4.4% and +6.8%, respectively (Figure 4F and 4I). In contrast, HE081 was different, whose $E_{95\%}$ and $E_{50\%}$ increased by +69.2% and +15.7%, respectively, compared to models of the original GTV (Figure 4, A and D), but $E_{5\%}$ increased only by +2.4% (Figure 4G). Both $SAR_{95\%}$ and $SAR_{50\%}$ demonstrated substantial increases by +223.0% and +80.6% (Figure 4, B and E), but the $SAR_{5\%}$ decreased by –3.4% (Figure 4H). A similar pattern was observed with current density PQMs, where the $CD_{95\%}$ and $CD_{50\%}$ increased by +71.2 and +27.1%, respectively (Figure 4, C and F), while the $CD_{5\%}$ decreased by <0.5% (Figure 4I). We could not expand the tumor from CS075 due to its proximity to the skull base. Regardless, this simulation using expansion models showed heterogeneity in PQM metrics between EY106 and HE081.

To further characterize the effect of changes in tumor volume, we eroded the GTV to simulate tumor shrinkage while keeping the skull defect constant. For EY106, $E_{95\%}$ increased by +18.1% compared to models of the original GTV

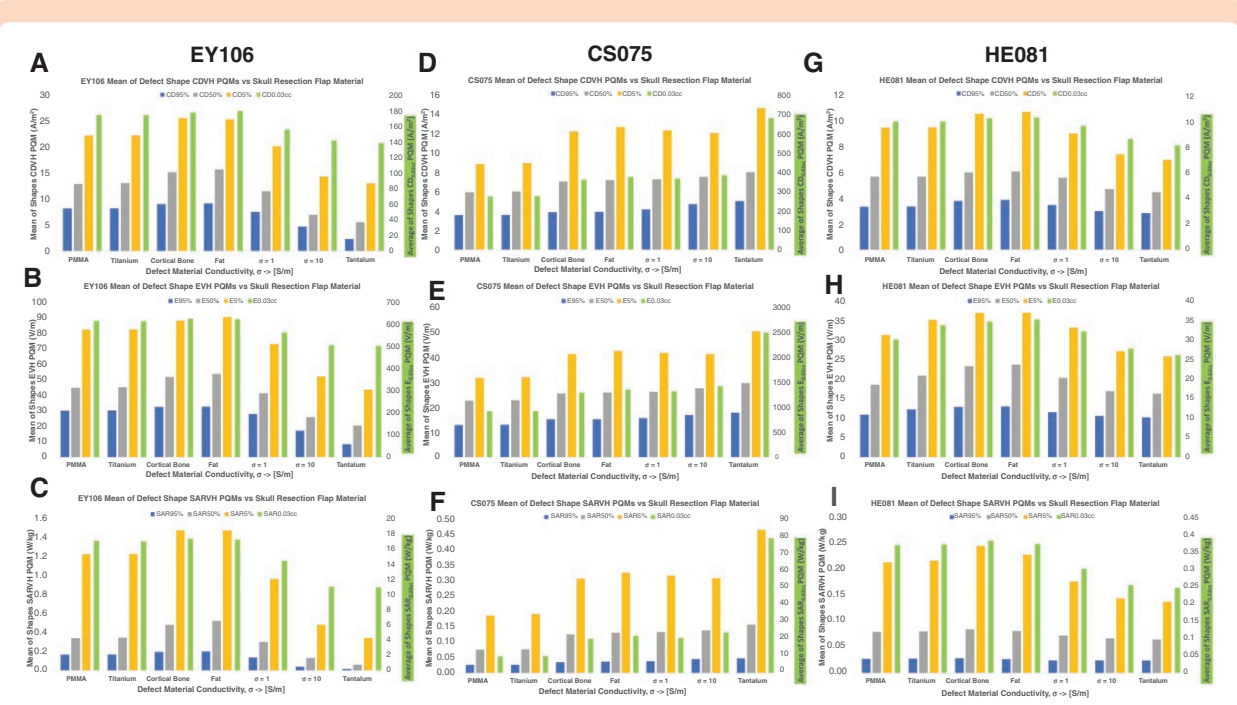

Figure 3. Plan quality metrics (PQM) and coverage statistics among various biomaterials. Mean PQM for current density volume histogram (CDVH) coverage with biomaterials having increasing conductivities for EY109 (A), CS075 (D), and HE081 (G). Mean PQM for electric field volume histogram (EVH) coverage with biomaterials having increasing conductivities for EY109 (B), CS075 (E), and HE081 (H). Mean PQM for specific absorption rate volume histogram (SARVH) coverage with biomaterials having increasing conductivities for EY109 (C), CS075 (F), and HE081 (I). Average PQM for 0.03 cc metrics is shown in green referenced to the right-sided secondary y-axis in each plot.

(Figure 4A), but both $E_{50\%}$ and $E_{5\%}$ decreased by –11.4% and –6.7%, respectively (Figure 4, D and G). We observed similar characteristics in SAR and current density. $SAR_{95\%}$ increased by +29.1%, while the $SAR_{50\%}$ and $SAR_{5\%}$ decreased by –23.5% and –6.5%, respectively (Figure 4, B, E, and H). The $CD_{95\%}$ increased by +14.1%, but both $CD_{50\%}$ and $CD_{5\%}$ decreased by –1.7% and –8.9%, respectively (Figure 4, C, F, and I). When eroded CS075 was compared with the original GTV model, $E_{95\%}$, $E_{50\%}$, and $E_{5\%}$ all decreased by –19.3%, –26.3%, and –33.7%, respectively (Figure 4, A, D, and G). The $SAR_{95\%}$, $SAR_{50\%}$, and $SAR_{5\%}$ all decreased by –27.1%, –44.4%, and –52.3%, respectively (Figure 4, B, E, and H). Similarly, $CD_{95\%}$, $CD_{50\%}$, and $CD_{5\%}$ all decreased by –3.4%, –28.6%, and –42.9%, respectively (Figure 4, C, F, and I). We did not erode the tumor from HE081 because it served as the reference volume for the erosion of EY106 and CS075. Nonetheless, the erosion models showed differences in PQM metrics between EY106 and CS075 indicating heterogeneity.

Discussion

Our study revealed several important findings pertaining to craniectomy defects in 3 particular glioblastoma patients and their relevance to TTFields treatment. First, the skull is an attenuator for electric field and the craniectomy defect in our index patient EY106 did not significantly increase TTFields coverage in GTV when the defect was modeled using cortical bone or fat. Their $E_{95\%}$, $E_{50\%}$, and $E_{5\%}$ were within a narrow range of 30, 40–50, and 80–90 V/m, respectively. Korshoej et al. examined circular craniectomies with diameters ranging from 10 to 100 mm in 5 mm increments above the glioblastoma, and they noted increased electric field strength with a diameter up to 50 mm and after which no further increase was observed.[15] EY106 had a craniectomy diameter of 74.7 mm and therefore the electric field penetration should be near the maximum for this particular patient. Consequently, we examined the defect geometry to determine if this affects TTFields coverage in the GTV. However, none of the geometries made a difference, with or without burr holes. We also virtually modeled a craniectomy defect in 2 additional patients, with the glioblastoma located in the occipital lobe in HE081 and the left inferior temporal lobe in CS075. Ultimately, we observed no noteworthy change in PQM metrics based on various geometries with or without burr holes, and this finding subsequently led us to consider the influence of biomaterial composition within the defect and the size ratio between GTV and the defect.

Certain biomaterials replacing the craniectomy defect yielded some of the largest changes in TTFields distribution in specific models. For the initial biomaterials tested (cortical bone, PMMA, titanium, and fat) with conductivity values of <1 S/m, they all facilitated higher electric field coverage for the GTV in EY106, while a similar effect was noted with a conductivity near 1 S/m for CS075 and a slightly smaller coverage was observed at <1 S/m for HE081. At higher conductivities of 1 and 10 S/m modeled as

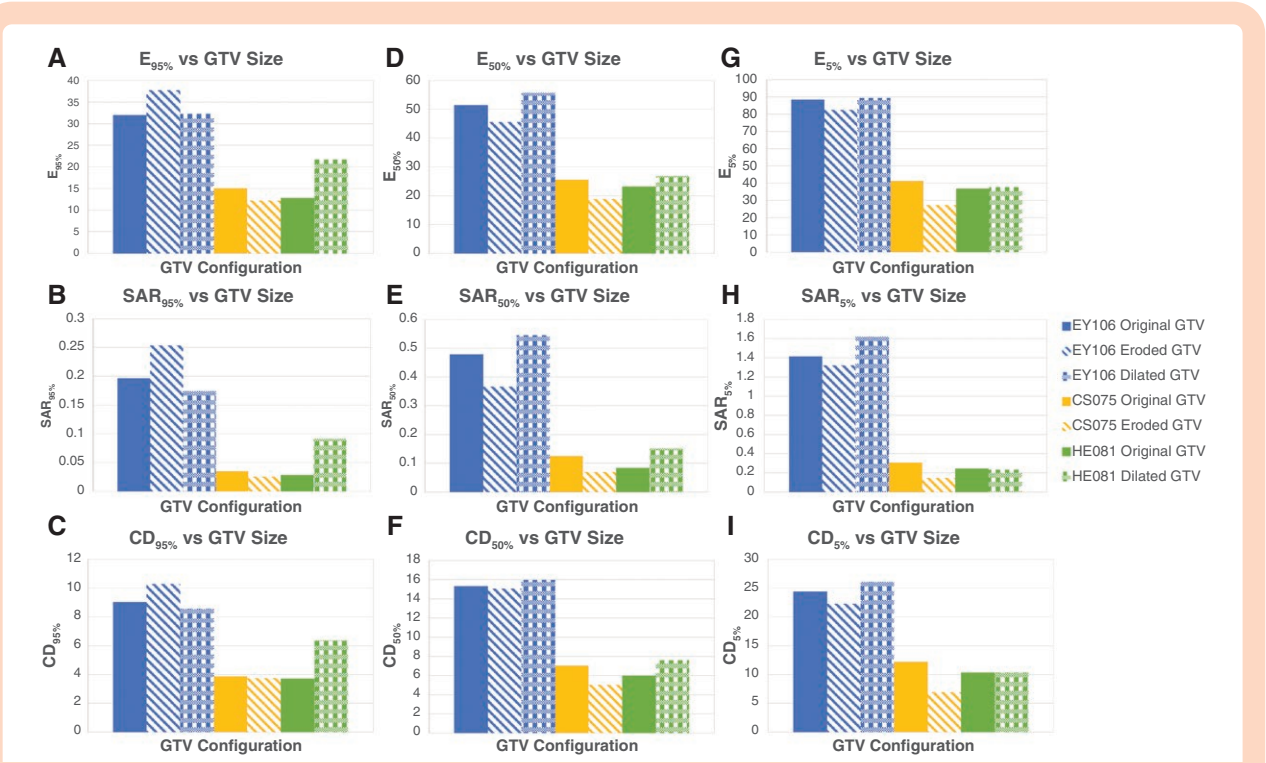

Figure 4. Heterogenous plan quality metrics (PQM) and coverage statistics among patients depending on gross tumor volume (GTV) size variations. Electric field PQM versus GTV size (A, D, and G). Specific absorption ratio PQM versus GTV size (B, E, and H). Current density PQM versus GTV size (C, F, and I). CS075 only has GTV erosion due to tumor location at the inferior margin of the left temporal lobe. HE081 only has expansion because the tumor was the designated reference minimum GTV size for this study.

virtual biomaterials, as well as 7.7×10^6 S/m in tantalum, all coverage statistics dropped for EY106 and HE081 but not for CS075. This drop in coverage statistics may be due to the tangential dispersion of electric fields on the convexity of the head in EY106 and HE081, and this property attenuated the fields penetrating perpendicularly into the brain. This is similar to transcranial direct current stimulation of the brain in which a circular electrode is better than a rectangular one due to the tangential dispersion of applied current and electric fields.[16] Furthermore, prior studies of craniectomy assigned scalp conductivity in the defect and noted an increase in TTFields coverage by +32.1% and +38.3% in frontal and temporal lobes, respectively.[15,17] This extension of the scalp into the defect may have overestimated the perpendicular component of penetrating electric fields. However, the tumor in CS075 is near the inferior margin of the head and dispersion may be limited due to fewer electrodes surrounding the virtual defect. In fact, tantalum helped increase coverage to the GTV in CS075 and this may be a result of electric current re-directed towards the GTV in a more perpendicular direction.[18] To the best of our knowledge, this is the first demonstration of the relevance of biomaterials within the craniectomy defect on TTFields coverage at the GTV. These findings have potential clinical implications because the choice of biomaterial may be important for TTFields treatment and thus await future validation in clinical trials.

We next investigated the relevance of the ratio between GTV and defect size and asked whether this ratio would alter TTFields coverage of the GTV. The expanded tumor in EY106 resulted in an increase of PQM metrics except for $SAR_{95\%}$ and $CD_{95\%}$, while HE081 also demonstrated an increase except for $SAR_{5\%}$ and $CD_{5\%}$. Remarkably, HE081 had a substantial increase in $E_{95\%}$, $SAR_{95\%}$, $SAR_{50\%}$, and $CD_{95\%}$ by +69.2%, +223.0%, +80.6%, and +71.2%, respectively. This substantial increase may be due to proximity of the expanded tumor near the surface of the brain where stronger electric fields can be found.[12] Furthermore, when the tumor was eroded, CS075 had a substantial decrease in all PQM metrics by –3.4% to –52.3%, while mixed increase and decrease were noted in EY106. The reduction in PQM metrics may be secondary to fewer electric field lines penetrating the eroded tumor. Together, this emphasizes the importance of individualizing TTFields delivery based on the size and location of the GTV. Unique array mapping coupled with finite element analysis of electric field distribution may enable personalized TTFields treatment and investigation in future clinical trials.

Conclusions

The geometry of the craniectomy defect alone, with or without burr holes, does not alter TTFields delivery to the glioblastoma GTV. However, the biomaterials filling the defect influence electric field penetration, and the ratio of GTV relative to defect size may enhance or attenuate TTFields coverage.

These findings are clinically relevant for personalized TTFields treatment.

Keywords

craniotomy | defect | glioblastoma | tumor-treating fields

Funding

This research was supported in part by the Musella Foundation for Brain Tumor Research and Information Inc.

Conflict of interest statement

E.T.W. received research grants from Novocure Ltd, Oblato Inc, and Orbus Therapeutics. E.T.W. reports a consulting relationship with Sumitomo Pharma Oncology Inc and Zai Lab Ltd. E.L. and E.T.W. have patent ##US 11,446,487 B2 issued to Beth Israel Deaconess Medical Center and patent #PCT/US2023/063368 pending to Rhode Island Hospital. E.T.W. served on data safety monitoring boards for Turning Point Therapeutics (now Bristol Myers Squibb) and OptimalTTF2 trial performed at Aarhus University Hospital. B.C., R.V., and M.H. have no disclosure.

Authorship statement

E.T.W., E.L., and M.H. developed the idea for this research investigation. RV was the brain tumor neurosurgeon and provided conceptual input. B.C., E.L., and E.T.W. performed computer modeling analyses. All authors helped write and review the manuscript. E.T.W. and E.L. supervised the work. Author responsible for statistical analysis: Edwin Lok, MS, Email: elok@bidmc.harvard.edu.

Data availability

The data used for this study will be made available upon reasonable request.

Affiliations

Brain Tumor Center & Neuro-Oncology Unit, Beth Israel Deaconess Medical Center, Boston, Massachusetts, USA (B.C., E.L., E.T.W.); Division of Hematology/Oncology, Department of Medicine, Brown University Health & Rhode Island Hospital, Providence, Rhode Island, USA (E.L., E.T.W.); Division of Neurosurgery, Department of Surgery, Beth Israel Deaconess Medical Center, Boston, Massachusetts, USA (R.V.); Department of Neurology, Beth Israel Deaconess Medical Center, Boston, Massachusetts, USA (M.H.); Departments of Neurology, Medicine, Neurosurgery & Radiation Oncology, Brown University Health & Rhode Island Hospital, Providence, Rhode Island, USA (E.T.W.)

References

1. https://www.accessdata.fda.gov/cdrh_docs/pdf10/p100034b.pdf. Accessed March 24, 2025.
2. https://www.accessdata.fda.gov/cdrh_docs/pdf10/P100034S013B.pdf. Accessed March 24, 2025.
3. Swanson KD, Lok E, Wong ET. An overview of alternating electric fields therapy (NovoTTF therapy) for the treatment of malignant glioma. *Curr Neurol Neurosci Rep.* 2016;16(1):8.
4. Stupp R, Taillibert S, Kanner A, et al. Effect of Tumor-Treating Fields plus maintenance temozolomide vs maintenance temozolomide alone on survival in patients with glioblastoma. *JAMA.* 2017;318(23):2306–2316.
5. Lacouture ME, Anadkat MJ, Ballo MT, et al. Prevention and management of dermatologic adverse events associated with tumor treating fields in patients with glioblastoma. *Front Oncol.* 2020;10:1045.
6. Gera N, Yang A, Holtzman TS, et al. Tumor treating fields perturb the localization of septins and cause aberrant mitotic exit. *PLoS One.* 2015;10(5):e0125269.
7. Karanam NK, Srinivasan K, Ding L, et al. Tumor-treating fields elicit a conditional vulnerability to ionizing radiation via the downregulation of BRCA1 signaling and reduced DNA double-strand break repair capacity in non-small cell lung cancer cell lines. *Cell Death Dis.* 2017;8(3):e2711.
8. Shteingauz A, Porat Y, Voloshin T, et al. AMPK-dependent autophagy upregulation serves as a survival mechanism in response to Tumor Treating Fields (TTFields). *Cell Death Dis.* 2018;9(11):1074.
9. Voloshin T, Kaynan N, Davidi S, et al. Tumor-treating fields (TTFields) induce immunogenic cell death resulting in enhanced antitumor efficacy when combined with anti-PD-1 therapy. *Cancer Immunol Immunother.* 2020;69(7):1191–1204.
10. Kirson ED, Dbaly V, Tovarys F, et al. Alternating electric fields arrest cell proliferation in animal tumor models and human brain tumors. *Proc Natl Acad Sci U S A.* 2007;104(24):10152–10157.
11. Timmons JJ, Lok E, San P, Bui K, Wong ET. End-to-end workflow for finite element analysis of tumor treating fields in glioblastomas. *Phys Med Biol.* 2017;62(21):8264–8282.
12. Lok E, San P, Hua V, Phung M, Wong ET. Analysis of physical characteristics of tumor treating fields for human glioblastoma. *Cancer Med.* 2017;6(6):1286–1300.
13. Lok E, Clark M, Liang O, et al. Modulation of Tumor-Treating Fields by cerebral edema from brain tumors. *Adv Radiat Oncol.* 2023;8(1):101046.
14. Wong ET, Lok E. Body fluids modulate propagation of tumor treating fields. *Adv Radiat Oncol.* 2024;9(1):101316.
15. Korshoej AR, Saturnino GB, Rasmussen LK, et al. Enhancing predicted efficacy of tumor treating fields therapy of glioblastoma using targeted surgical craniectomy: A computer modeling study. *PLoS One.* 2016;11(10):e0164051.
16. Datta A, Bansal V, Diaz J, et al. Gyri-precise head model of transcranial direct current stimulation: Improved spatial focality using a ring electrode versus conventional rectangular pad. *Brain Stimul.* 2009;2(4):201–7, 207.e1.
17. Jin T, Dou Z, Zhao Y, et al. Skull defect increases the tumor treating fields strength without detrimental thermogenic effect: A computational simulating research. *Cancer Med.* 2023;12(2):1461–1470.
18. Lok E, Wong ET. Body fluids modulate propagation of tumor treating fields. *Adv Radiat Oncol.* 2023;9(1):101316.